Genetic dissection of Rift Valley fever pathogenesis:

Rfvs2 on mouse chromosome 11 enables survival to acute-onset hepatitis

Leandro Batista,[1,2] Gregory Jouvion,[4,5] Dominique Simon-Chazottes,[1,3] Denis Houzelstein,[1] Odile Burlen-Defranoux,[6] Magali Boissière,[7] Satoko Tokuda,[1] Tania Zaverucha Do Valle,[1,8] Ana Cumano,[6] Marie Flamand,[7] Xavier Montagutelli,[1,3¶*] & Jean-Jacques Panthier[1¶]

[1] Mouse Functional Genetics, Institut Pasteur, UMR3738, CNRS, Paris 75015, France
[2] Sorbonne Université, IFD, Paris 75005, France
[3] Mouse Genetics, Institut Pasteur, Paris 75015, France
[4] Experimental Neuropathology, Institut Pasteur, Paris 75015, France.
[5] Sorbonne Université, INSERM, Physiopathologie des Maladies Génétiques d'Expression Pédiatrique, APHP, Hôpital Armand Trousseau, UF de Génétique Moléculaire, Paris 75012, France
[6] Lymphopoiesis, Institut Pasteur, U668, INSERM, Paris 75015, France
[7] Structural Virology, Institut Pasteur, Paris 75015, France
[8] Laboratório de Imunomodulação e Protozoologia, Instituto Oswaldo Cruz, Fiocruz, Rio de Janeiro, Brasil

*Corresponding author

E-mail: xavier.montagutelli@pasteur.fr (XM)

[¶] These authors contributed equally to this work.

Short title: A single locus enables survival to Rift Valley fever hepatitis

Abstract

The systemic inoculation of mice with Rift Valley fever virus (RVFV) reproduces major pathological features of severe human disease, notably the acute-onset hepatitis and delayed-onset encephalitis. We previously reported that a genomic interval (*Rvfs2*) derived from the susceptible MBT/Pas strain is associated with reduced survival time after RVFV infection. In this study, we investigated the pathophysiological mechanisms by which *Rvfs2* confers increased susceptibility to BALB/c mice that are congenic for *Rvfs2* (C.MBT-*Rvfs2*) after infection with virulent RVFV. Clinical traits, biochemical parameters, and histopathological features indicated similar liver damage in BALB/c and C.MBT-*Rvfs2* mice between the third and fifth days after infection. However, C.MBT-*Rvfs2* mice died at that point from acute liver injury while most BALB/c mice recovered from this condition but eventually died of encephalitis. We observed that hepatocytes proliferated actively within the infected liver of BALB/c mice on the sixth day after infection, promoting organ regeneration on the eighth day after infection and recovery from liver damage. We found that the production of infectious virions was up to 100-fold lower in the peripheral blood and liver of BALB/c compared to C.MBT-*Rvfs2* mice. Likewise, RVFV protein amounts were much lower in BALB/c liver compared to C.MBT-*Rvfs2* liver. Primary cultured hepatocytes showed higher viral replication rate in C.MBT-*Rvfs2* which could contribute to the susceptibility conferred by *Rvfs2*. Using bone marrow chimera experiments, we uncovered that both hematopoietic and non-hematopoietic cells are required for the BALB/c allele of *Rvfs2* to exert its protective effects against the RVFV-induced acute liver disease. Taken together, we have established that *Rvfs2* acts as an important RVFV restriction factor by limiting virus multiplication in mice.

Author Summary

Rift Valley fever (RVF) is a mosquito-borne viral disease with potential to generate a public health emergency. The wide variation in RVF symptoms and severity observed within patient population suggests that natural host genetic determinants, among other factors, can influence the disease outcome. Infection of mice mimics several features of the pathology in humans, including acute-onset hepatitis and delayed-onset encephalitis. BALB/c inbred mice bearing the BALB/c haplotype at the *Rvfs2* locus survive longer than those bearing the MBT haplotype. In this study, we investigated clinical traits, biochemical parameters, virological evidence, and histological features to characterize the pathogenesis of RVF in early and late susceptible mice. We show that animals of both groups develop acute liver disease shortly after infection. We demonstrate that, by comparison with early susceptible mice, BALB/c mice exhibit significantly reduced replication of RVF virus *in vivo* in the blood and liver and *in vitro* in primary cultured hepatocytes, and eventually self-recover from the liver damages. We use reciprocal transplantations of bone marrow cells between early and late susceptible mice to show that survival to severe liver disease requires both hematopoietic and non-hematopoietic cells. Taken together, we establish *Rvfs2* as a single locus that enables mice to survive RVF virus-induced liver disease.

Introduction

Rift Valley fever (RVF) is a mosquito-borne viral disease with potential to generate a public health emergency [1]. In humans, infection leads to a great variety of clinical manifestations that range from a febrile influenza-like illness to hepatitis with fatal hemorrhagic fever, encephalitis and retinitis [2, 3]. In ruminant species, a wide variation in susceptibility to RVF disease is observed among different individuals. Some infected animals suffer from unapparent or moderate febrile reactions while others develop high fevers and severe prostration, which may lead to death in the most susceptible animals [4-6]. Sequence analysis of RVF virus (RVFV) strains collected during the 1977-1979 Egyptian outbreak has shown that, although all virus isolates carried virtually identical genotypes, remarkable differences were observed in pathogenesis across human and animal populations [7]. These findings suggest that the different pathogenic phenotypes were not linked to specific mutations in the viral genome but could rather be caused by variations in dose and route of virus exposure and by host-related factors including age, sex, overall immune response, nutritional status and genetic variants.

Careful control of experimental conditions of infection in rodent models have helped establishing host genetic factors as important determinants in RVF disease severity. The infection of laboratory rodents mimics several features of RVFV-induced pathology in humans, including hepatitis with liver necrosis and meningoencephalitis [8, 9]. The first rat models consisted of the Wistar-Furth (WF) inbred strain which is highly susceptible to the hepatitis induced by subcutaneous inoculation with RVFV, while the Lewis (LEW) strain is largely resistant [8, 10]. Notably, WF rats were not uniformly susceptible to different RVFV strains [11]. Inhalation exposure to RVFV confirmed the extreme susceptibility of the WF strain to RVFV-induced hepatitis [12]. The segregation analysis of the RVFV susceptible

92 phenotype in LEW and WF backcrosses suggested a simple Mendelian dominant control [10].
93 A WF.LEW congenic strain resistant to the fatal hepatitis was created by repeated
94 backcrosses from the resistant LEW to the WF susceptible genetic background [13]. A single
95 region on rat chromosome (Chr) 3 was shown to significantly increase the survival rate of
96 animals carrying the LEW haplotype [14] but the gene accounting for this improved
97 resistance has yet to be identified.
98 Mouse inbred strains also exhibit differences in their susceptibility to an infection with
99 RVFV. In one study, the subcutaneous infection of BALB/c mice with 10^3 plaque-forming
100 units (PFU) of the ZH501 RVFV strain led to an extensive infection of the liver [9]. The
101 resulting liver disease accounted for the death of most animals between days 3 and 6 post
102 infection (p.i.). Mice that survived this early liver disease later developed encephalitis and
103 died around day 8 p.i. [9]. In another study, C57BL/6 mice appeared more susceptible than
104 BALB/c mice under similar experimental conditions and succumbed to acute liver disease
105 within 4 days [15]. We have tested the susceptibility of additional strains derived from
106 various *Mus musculus* subspecies trapped in the wild. The most severely affected strain
107 within this collection, MBT/Pas (MBT), developed very early onset RVF disease. After
108 intraperitoneal infection with 10^2 PFU of virulent RVFV strain, either Egyptian ZH548 or
109 Kenya 98, MBT mice died more rapidly than BALB/c or C57BL/6 mice [16]. It is worth
110 noting that MBT mice are susceptible to RVFV but resistant to several other viruses [16],
111 suggesting that the susceptibility to RVFV exhibited by MBT mice is not attributable to
112 generalized immunodeficiency. In flow cytometry studies, we have recently shown that MBT
113 mice displayed several immunological alterations after RVFV infection. Furthermore, these
114 mice failed to prevent high viremia and viral antigen loads in the blood, spleen, and liver [17].
115 We also showed that, in MBT mice, RVF susceptibility is inherited in a complex polygenic
116 fashion and we identified three genomic intervals on Chr 2, 11 and 5 affecting survival time

after RVFV infection. Each of these MBT-derived intervals, designated Rift Valley fever susceptibility 1 (*Rvfs1*), *Rvfs2* and *Rvfs3* respectively, conferred reduced survival time in C.MBT congenic strains in which these intervals had been transferred onto the less susceptible BALB/c genetic background [18]. The pathogenic mechanisms for the early death induced by RVFV in the C.MBT congenic strains are currently unknown.

In this study, we investigated the phenotypic features associated with morbidity in BALB/c mice congenic for the MBT-derived *Rvfs2* interval, i.e. C.MBT-*Rvfs2* mice. We focused our investigations on male mice which exhibit slightly higher susceptibility to RVFV infection [18]. The study of clinical, biochemical and virological parameters, as well as histopathological features of the RVF disease showed that mice from both BALB/c and C.MBT-*Rvfs2* inbred strains exhibited hepatic disease. The first clinical signs of disease were detected on the third day of infection in both strains. However, while C.MBT-*Rvfs2* mice began to die on day 4 of acute liver disease, most BALB/c mice recovered and died three to nine days later of encephalitis. Since MBT-derived *Rvfs2* allele was associated with increased viral load in the liver and higher viral replication rate in primary cultured hepatocytes, we conclude that the death of C.MBT-*Rvfs2* mice is due to enhanced susceptibility to the acute-onset, RVFV-induced liver disease. Reciprocal transplantations of bone marrow cells between BALB/c and C.MBT-*Rvfs2* mice showed that both hematopoietic and non-hematopoietic cells are required for the capacity of BALB/c mice to survive liver damages.

Results

BALB/c and C.MBT-*Rvfs2* mice have evidence of liver disease at the early stage of infection

C.MBT-*Rvfs2* congenic mice carry a ≈17 Mb segment of chromosome 11 region from the MBT strain on the BALB/c background (Fig 1A) [18]. The challenge of C.MBT-*Rvfs2* mice with 10^2 PFU of the ZH548 RVFV strain showed that *Rvfs2* has a strong effect on susceptibility to RVFV. More than 50% of C.MBT-*Rvfs2* mice died within 4 days after infection with RVFV, whereas half of BALB/c mice survived for over 8 days (Mantel-Cox's Logrank test, $P<0.0001$) (Fig 1B).

Clinical signs of disease in RVFV-infected C.MBT-*Rvfs2* mice were monitored daily in comparison with BALB/c in order to explore the causes of this increased susceptibility. C.MBT-*Rvfs2* mice developed signs of an acute disease with ruffled fur, hunched appearance and lethargy as early as days 3 and 4 p.i. In contrast, most RVFV-infected BALB/c mice exhibited the first symptoms of disease later, from day 6 p.i. BALB/c mice showed different degrees of disorders, including ascending paralysis, ataxia, head-tilt and circling behavior. These clinical observations suggest that distinct presentations of the disease are controlled be the introgressed chromosomal region.

Quantitative clinical traits and biochemical parameters associated with the health status were recorded to further characterize differences in disease progression between BALB/c and C.MBT-*Rvfs2* mice. Body weight and body temperature were measured daily in RVFV-infected mice from both strains. On average, BALB/c mice lost body weight on days 3 and 4, and from day 7 to day 9 p.i. Between these two intervals their body weight remained stable. By contrast, C.MBT-*Rvfs2* mice lost weight rapidly from day 3 p.i. until their death (Fig 2A). No differences were found between the two strains in body weight loss at days 3 and 4 (two-

161 way ANOVA, P(strain effect)=0.54). Temperature measurements indicated that neither
162 BALB/c nor C.MBT-*Rvfs2* mice became febrile during the course of infection. A significant
163 drop in body temperature was observed one day before death in both inbred strains, regardless
164 of the cause of death (Fig 2B). Overall, no differences in body temperature between BALB/c
165 and congenic mice were found (two-way ANOVA, P(strain effect)=0.69). As RVFV is known
166 to be a hepatotropic virus [19], blood levels of liver enzymes were measured during the
167 disease course in uninfected and infected BALB/c and C.MBT-*Rvfs2* mice. Alanine
168 aminotransferase (ALT) and aspartate transaminase (AST) peaked on day 4 p.i. in both
169 infected strains (Fig 2C and 2D), indicating hepatocyte damage. After day 5 p.i., AST and
170 ALT serum levels decreased slowly in infected BALB/c mice and returned to normal levels
171 on day 8 p.i., suggesting recovery from the liver disease. Altogether the development of the
172 RVF disease in the first 4 days was similar in both inbred strains.

173 **BALB/c and C.MBT-*Rvfs2* mice exhibit liver damage at days 3 and 4 p.i.**

174 We studied in further detail the tissue damage caused by RVFV in the liver of infected
175 BALB/c (N=10) and C.MBT-*Rvfs2* (N=8) mice euthanized on day 3 p.i. Histopathological
176 analyses of the liver revealed three different lesion profiles of increasing severity in both
177 mouse genotypes (Fig 3). Five out of 10 BALB/c and 5/8 C.MBT-*Rvfs2* mice exhibited mild,
178 multifocal and well demarcated lesions defined as Profile 1. Liver lesions in these mice were
179 characterized by hepatocyte cell death associated with small inflammatory infiltrates
180 containing fragmented neutrophils (Fig 3A and 3B). Immunohistochemical (IHC) labeling
181 directed against the viral N protein was used to identify infected cells (note that the technique
182 used could not provide quantitative information on the infection level in infected cells). This
183 analysis revealed small multifocal foci (less than 100 µm in diameter) of infected hepatocytes
184 (Fig 3C). Profile 2 was observed in 3/10 BALB/c and 2/8 C.MBT-*Rvfs2* mice. This profile
185 was also characterized by multifocal lesions with hepatocyte cell death. However, lesions

were more severe, extensive and diffuse (Fig 3D and 3E). IHC analyses detected a stronger signal with slightly larger foci of infected hepatocytes (Fig 3F). A third profile was observed in 2/10 BALB/c and 1/8 C.MBT-*Rvfs2* mice. Liver sections categorized as Profile 3 displayed severe and diffuse tissue damage without signs of inflammation. Lesions were characterized by acute and massive cell death of hepatocytes, numerous viral inclusion bodies in the nuclei of cells (Fig 3G and 3H), and a diffuse positive immunolabeling of hepatocytes for the viral N protein (Fig 3I). None of these lesions were observed in liver sections of uninfected BALB/c and C.MBT-*Rvfs2* mice. Collectively, these results indicated that BALB/c and C.MBT-*Rvfs2* mice experienced similar liver conditions on day 3 p.i. with the same range of histological lesions, from mild to severe, up to extensive destruction of the liver parenchyma. Overall, non-quantitative IHC indicated, in each profile, similar amounts of RVFV-infected liver cells in both strains.

We then examined the liver of moribund C.MBT-*Rvfs2* mice in order to provide further histological evidence of disease progression. Five congenic mice were euthanized when exhibiting clinical signs of severe disease, on days 3 (N=1), 4 (N=2) and 4.5 (N=2) p.i. All five livers displayed severe and non-inflammatory lesions, characterized by massive and acute cell death. These observations resembled closely those described above as Profile 3 (not shown), supporting the hypothesis that, in C.MBT-*Rvfs2* mice, the disease progressed from mild inflammation to non-inflammatory liver lesions with extensive tissue damage. Lesions observed in the liver of moribund C.MBT-*Rvfs2* mice were sufficient to alter liver function, leading to the rapid death of infected animals.

Infected BALB/c mice survive the early-onset liver disease, but succumb later to encephalitis

The gradual decrease of liver transaminases between days 5 and 8 post-infection in BALB/c mice suggested hepatic tissue regeneration. We further evaluated the extent of liver recovery,

211 by examining histopathological changes in livers of moribund BALB/c mice (N=4)
212 euthanized between day 6 and 9 p.i. (Figs 4 and 5). On day 6 p.i., only minimal lesions were
213 observed (Fig 4A and 4B) and few RVFV N-positive hepatocytes were detected (Fig 4C). An
214 increased number of mitosis as well as a strong and diffuse expression of Ki67 confirmed the
215 proliferation of hepatocytes (Fig 4D). By day 8, minimal to mild, subacute to chronic
216 inflammatory lesions were scattered in the liver parenchyma or centered on portal tracts and
217 consisted of small infiltrates of lymphocytes, plasma cells and macrophages (Fig 5A and 5B).
218 Very few hepatocytes were labeled positively for the RVFV N protein, confirming an
219 efficient viral clearance in the hepatic tissue (Fig 5C). Since BALB/c mice exhibited clinical
220 neurological signs, we investigated their brain for infection-related lesions. Histopathological
221 lesions were visible in the brain of moribund BALB/c mice. The virus targeted different brain
222 anatomic structures in each individual mouse, and no pathognomonic lesion profile could be
223 defined (Fig 5D-I). We detected (i) subacute leptomeningitis with multifocal infiltration of the
224 leptomeninges by lymphocytes, plasma cells, and neutrophils (Fig 5D), and (ii) cell death foci
225 in different locations of the cerebral grey matter, e.g. the outer granular layer or different
226 brain nuclei (Fig 5E, 5F, and 5G). In these foci, shrinkage of neurons, gliosis, infiltration of
227 neutrophils and strong RVFV N protein immunolabeling of neurons were observed (Fig 5H
228 and 5I). These lesions were likely the cause of the neurological symptoms and eventual death
229 in BALB/c mice.

230 **Elevated viral burden in the blood and liver of C.MBT-*Rvfs2* mice**

231 In order to assess differences in the viral production, we first measured the titer of infectious
232 viral particles in the blood and liver of BALB/c and C.MBT-*Rvfs2* mice on day 3 p.i. by
233 standard plaque assay. The viral titers were about 80- and 100-fold higher in the
234 C.MBT-*Rvfs2* blood and liver, respectively, compared with those found in BALB/c mice
235 (Mann Whitney-U test, $P<0.001$ and $P=0.016$, respectively; Fig 6A and 6B). Finally, semi-

quantitative protein analysis of liver extracts at day 3 p.i. by Western blot indicated that high levels of N nucleocapsid and NSs nonstructural viral proteins were found in the liver of C.MBT-*Rvfs2*, while both viral proteins were undetectable in BALB/c liver (Fig 6C) despite the same proportions of RVFV-infected cells in the two strains revealed by IHC (Fig 3). Altogether, these results indicated that, compared to BALB/c mice, C.MBT-*Rvfs2* mice have reduced ability to limit the replication of RVFV thus allowing the production of the virus systemically and specifically in the liver at much higher levels.

Increased viral replication in C.MBT-*Rvfs2*-derived cultured primary hepatocytes

To further analyze the increased susceptibility of C.MBT-*Rvfs2* mice to RVFV-induced liver disease, we derived primary cultured hepatocytes from the liver of BALB/c and C.MBT-*Rvfs2* uninfected mice. We measured the kinetics of viral production in the culture medium over 60 h after infecting hepatocytes with RVFV. While the viral titer remained constant at 300-400 PFU/ml in the BALB/c culture, it peaked in C.MBT-*Rvfs2*-derived hepatocytes at almost 900 PFU/ml 24h after infection before decreasing at 48 and 60 hours post-infection (Fig 7). This increased viral replication in C.MBT-*Rvfs2* hepatocytes is likely one of the mechanisms responsible for the enhanced susceptibility to the liver disease conferred by the *Rvfs2* locus.

Both hematopoietic and non-hematopoietic cells are required for *Rvfs2*-dependent survival to liver disease

We have recently shown that the inbred strain MBT displays multiple immune-related defects in response to RVFV infection [17]. Together with transcriptomics data from a previous study [16], these results suggest that innate immune cells might be the critical determinant for survival to liver disease. To test this hypothesis, we produced chimeric mice using crosswise transplantations of bone-marrow cells after total body irradiation to evaluate whether the effects of *Rvfs2* in hematopoietic cells, in non-hematopoietic cells, or in both were required for survival to the RVFV-induced liver disease. We generated BALB/c mice reconstituted

261 with C.MBT-*Rvfs2* marrow (C.MBT-*Rvfs2* → BALB/c chimeras) and C.MBT-*Rvfs2* mice
262 reconstituted with BALB/c marrow (BALB/c → C.MBT-*Rvfs2* chimeras). Controls consisted
263 of irradiated mice reconstituted with isogenic marrow, (BALB/c → BALB/c and
264 C.MBT-*Rvfs2* → C.MBT-*Rvfs2* chimeras). After reconstitution, the mice were infected with
265 RVFV. As shown in Figure 8, BALB/c → BALB/c mice survived significantly longer than
266 C.MBT-*Rvfs2* → C.MBT-*Rvfs2* mice (Mantel-Cox's Logrank test, P=0.0002), like the non-
267 manipulated BALB/c and C.MBT-*Rvfs2* strains (Fig 1B). Interestingly, the survival time was
268 significantly shorter in C.MBT-*Rvfs2* → BALB/c mice compared to BALB/c → BALB/c
269 mice (Mantel-Cox's Logrank test, P<0.01), suggesting that bone marrow-derived cells are
270 needed to confer prolonged survival in BALB/c mice. However, the survival time of
271 BALB/c → C.MBT-*Rvfs2* mice was not increased compared to
272 C.MBT-*Rvfs2* → C.MBT-*Rvfs2* mice (Mantel-Cox's Logrank test, P=0.78), suggesting that
273 bone marrow-derived cells from BALB/c mice alone are not sufficient to confer the BALB/c
274 phenotype to C.MBT-*Rvfs2* mice. Together, these results suggest that the *Rvfs2* effects in both
275 hematopoietic and non-hematopoietic compartments are critical for survival to the early-onset
276 liver disease in RVFV-infected mice.
277

Discussion

There is considerable variability in the ability of patients and livestock to survive RVF disease. A number of factors, such as the viral strain, the route and dose of viral exposure and the age, sex, nutritional and immune status of the host, can modulate the severity of the disease and contribute to the balance between recovery and death, a complex phenotype that involves multiple systems, organs, tissues, immune cells and cellular pathways, under the influence of multiple genes. The importance of inoculation route and dose and of the age and sex of the host has been experimentally demonstrated in laboratory rodents [10, 12, 13, 16, 20]. Experiments in laboratory rodents have further demonstrated that survival time and survival rate following RVFV infection are influenced by host genetic determinants [10, 16]. Our previous studies have shown that susceptibility to RVF in the inbred MBT mouse strain is inherited in a complex fashion, with sex influencing the severity of the disease. Three RVF susceptibility loci (*Rvfs*) with a moderate effect on the survival time were identified [18]. The introgression by repeated backcrosses of each of these chromosomal regions within the less susceptible genetic background BALB/c led to congenic mice exhibiting significant reduction in survival time compared to the BALB/c control groups [18]. Functional studies are needed to unravel the nature and the role of the genes within the *Rvfs* loci in the pathogenesis of RFV. We chose to focus our efforts first on *Rvfs2*, a 17Mb genomic interval, because of its strongest effect.

In our mouse model, the animals are infected by intraperitoneal injection of 10^2 PFU of the ZH548 RVFV strain [2, 21]. This virus dose was initially chosen to induce high mortality in both MBT and BALB/c parental strains (S1 Table). In these conditions, most MBT mice died within 5 days p.i. with the clinical signs of liver disease. By contrast, most BALB/c mice lived beyond that date and exhibited signs of encephalitis, such as paralysis, ataxia, or head-

tilting behavior [16]. Notably, the difference in the days of death between BALB/c and MBT mice was identical at infectious doses ranging from 10 to 1000 PFU (S1 Table).

The pathogenesis induced by the subcutaneous challenge of BALB/c mice with 10^3 PFU ZH501 RVFV has been recently characterized in detail [9, 22]. Approximately 80% of BALB/c mice infected in these conditions were reported to have succumbed with severe liver disease between days 3 and 6 p.i., a much higher percentage than the one observed in our study (<10%). Several experimental factors differ between the two studies. Although ZH501 and ZH548 RVFV strains have been isolated in the same hospital during the 1977 Egyptian outbreak, they have distinct passaging history [9] and exhibit a small percentage of nucleotide differences [7, 21, 23]. Therefore, we cannot exclude that ZH501 and ZH548 RVFV strains induce distinct survival rates at day 6 p.i. Based on our previous experiments (S1 Table), a lower inoculation dose (10^2 instead of 10^3 PFU) is unlikely to be solely responsible for a reduced death rate between days 3 and 6 p.i. in our study. Finally, this difference could be due to mouse sex and genetic background since we used males of the BALB/cByJ inbred strain while the other study was performed on female BALB/c mice, without indication of the substrain. Significant differences between BALB/c substrains have been previously reported with other infectious diseases and immune responses [24, 25], emphasizing the importance of accurately specifying the animal strain used is such studies. Whatever the reason for this difference in survival rates, our findings are consistent with the biphasic RVF disease reported by Smith and colleagues [9] that consists of an acute liver disease followed by a panencephalitis.

Under our conditions, C.MBT-*Rvfs2* mice were highly susceptible to, and died from, the early-onset liver disease, while BALB/c mice overcame it and died later of encephalitis. Our results suggest that one of the mechanisms underlying the increased susceptibility of C.MBT-*Rvfs2* mice is a higher viral replication rate at the cellular level, as shown in primary

cultured hepatocytes and by the increased viral load in the liver, despite similar percentage of infected liver cells as assessed by non-quantitative IHC. Altogether, these findings establish the feasibility and exemplify the value of segregating important sub-phenotypes by transferring a single locus, *Rvfs2,* from the early susceptible to a late susceptible background. Susceptibility to liver disease has also been reported in WF inbred rats after subcutaneous infection with RVFV ZH501 [8]. WF rats died by day 2 post inoculation of liver necrosis, whereas LEW rats were resistant to the liver disease but fairly susceptible to the encephalitis [8, 13]. This susceptibility to liver necrosis occurred in a similar time frame after respiratory infection in WF rats [12]. The pathogenic mechanisms that trigger the susceptibility of WF rats and C.MBT-*Rvfs2* mice to RVF hepatic disease may be similar. Indeed, it has been reported that susceptible WF rats had much higher blood viral titers than resistant LEW rats at day 2 p.i. [13], in line with the higher viral production in hepatocytes from WF rats compared with LEW rats [26]. These data suggest that the rat susceptibility locus also controls the production of RVFV. Recently, a major gene for the susceptibility has been mapped within a region on rat Chr 3 [14]. This rat region has homology with mouse Chr 2, indicating that the rat susceptibility locus and *Rvfs2* which maps on mouse Chr 11 do not point at the same gene(s). Therefore, the genetic variations captured in WF rats and MBT mice are different, which makes both rodent models equally interesting and important.

In principle, the RVFV-infected host can protect itself from lethal liver disease using two non-mutually exclusive strategies: (i) resistance to reduce viral burden, (ii) tolerance to reduce the negative impact of the viral burden on host fitness [27, 28]. Our study indicates that the main contributor to early lethality of C.MBT-*Rvfs2* mice can be attributed to higher levels of RVFV in the blood and liver and higher viral replication rate in hepatocytes compared to BALB/c mice. Whether higher susceptibility to liver disease is only due to lower resistance or also to reduced tolerance remains to be determined. The distinct overall phenotype of the

352 BALB/c → BALB/c chimeras compared with the BALB/c → C.MBT-*Rvfs2* and
353 C.MBT-*Rvfs2* → C.MBT-*Rvfs2* chimeras demonstrated an absolute requirement of both
354 BALB/c hematopoietic and BALB/c non-hematopoietic cells for *Rvfs2*-induced resistance.
355 Previous work, including ours, have revealed the importance of specific genetic regions in the
356 outcome of RVFV infection. This report provides insight into the role of the *Rvfs2* locus. Host
357 genetic factors may influence multiple pathways or molecular or cellular processes, such as
358 the production of virus by infected cells or the immune responses. Our previous work has
359 unraveled an impaired innate immune response in MBT mice [16] as well as other
360 immunological differences [17]. Other studies have emphasized the role of cytokines and T-
361 cell responses in the pathogenesis of RVF disease [29, 30]. The causal variants within the 17
362 Mb *Rvfs2* genomic interval remain to be identified, as well as the mechanisms by which they
363 control the production of infectious virus particles and the ability to survive the RVF-induced
364 liver disease.
365

Materials and Methods

Ethics statement

Experiments on mice were conducted according to the French and European regulations on care and protection of laboratory animals (EC Directive 2010/63/UE and French Law 2013-118 issued on February 1, 2013). All experimental protocols were approved by the Institut Pasteur Ethics Committee (under #2013-0127, 2016-0013 and dap160063) and authorized by the French Ministry of Research (under #02301, 06463 and 14646, respectively).

Mice

C.MBT-(JAX0003137-UNC20541010) congenic mice, designated herein as C.MBT-*Rvfs2*, carry a segment of Chr 11 from the MBT/Pas (MBT) inbred strain extending between positions 104,823,629 and 121,738,604 in assembly mapping GRCm37, onto a BALB/cByJ (BALB/c) inbred genetic background [18]. C.MBT-*Rvfs2* and BALB/c mice were bred under specific pathogen-free conditions at the Institut Pasteur.

Virus production and mouse infection

The RVFV strain ZH548, isolated from a male patient with the acute febrile illness at Zagazig fever hospital, Egypt [21, 31] (obtained from Centre National de Référence des Fièvres Hémorragiques Virales, Institut Pasteur, Lyon, France), was used for all infection studies. All experiments that involved virulent RVFV were performed in the biosafety level 3 (BSL3) facilities of the Institut Pasteur, and carried out in compliance with the recommendations of the Institut Pasteur Biosafety Committee (N° 14.320). Stocks of RVFV ZH548 were titrated by plaque assay on monolayers of Vero E6 cells [32]. Infections were carried out on 9 to 13 weeks old male mice, in BSL-3 isolators. Mice were infected intraperitoneally with 10^2 PFU of RVFV strain ZH548. Clinical disease scores and mortality were monitored daily for 14

days following infection. Moribund animals were euthanized. Animals that survived were euthanized on the last day of the monitoring period.

Clinical evaluation

Implantable Programmable Temperature Transponders (IPTT-300) (Bio Medic Data Systems, Inc., Seaford, DEL, USA) were injected subcutaneously into mice one week prior to challenge with RVFV ZH548, and body temperature was monitored daily. Body weight of ZH548-infected mice was measured daily throughout the course of the experiment to evaluate the daily weight loss. Alanine aminotransferase (ALT) and aspartate aminotransferase (ALT) levels were measured using IDEXX diagnostic panels analyzed on a VetTest chemistry analyzer (IDEXX laboratories, Westbrook, ME, USA) on ZH548-infected mice and uninfected controls.

Viral titer, viral RNA load, and expression of N and NSs viral proteins

Groups of infected BALB/c and C.MBT-*Rvfs2* mice were euthanized on day 3 p.i. Blood was collected by cardiac puncture. The left lateral lobe of the liver was harvested after perfusion from the portal to the cava vein with saline to remove blood-associated RVFV from the tissues. Infectious titers were measured in sera samples and liver homogenates by plaque assay on monolayers of Vero E6 cells [32].

The expression of N and NSs viral proteins was studied by Western blot analysis. Total proteins were extracted from liver samples of two mice used above for viral titration (noted b1, b2, r1 and r2 on figure 6). Protein quantification was done using Micro BCA Protein Assay kit (ThermoFisher Scientific, Waltham, MA). Ten µg of total protein from a cell lysate from AML12 hepatocytes infected with RVFV at an MOI of 3 were used as a positive control. Forty micrograms of total proteins extracted from liver samples and resuspended in Laemmli buffer were run on 14% SDS-polyacrylamide gel and transferred onto nitrocellulose membranes (Amersham, Velizy-Villacoulay, France). Membranes were blocked with a

414 solution of 5% milk (low fat) in PBS containing 0.05% of Tween 20 also used to dilute
415 antibodies (Ab). Proteins were detected by using a rabbit polyclonal Ab raised against a
416 recombinant N protein produced in the baculovirus system, a mouse polyclonal Ab raised
417 against the entire NSs protein [33, 34], or a monoclonal anti-β-actin antibody (A5441, Sigma-
418 Aldrich, Saint-Quentin Fallavier, France). The membranes were incubated with anti-rabbit or
419 anti-mouse Ab coupled to horseradish peroxidase (Sigma-Aldrich,) then reacted with a
420 chemiluminescent substrate (SuperSignal West Dura Extended Duration Substrate, Thermo
421 Scientific), and revealed with G:BOX Chemi chemiluminescence imaging system (Bangalore,
422 India).

423 **Histology and immunostaining**

424 Groups of infected BALB/c and C.MBT-*Rvfs2* mice were euthanized at different times along
425 the 14-day period of observation to monitor the development of RVF disease. A first group
426 was euthanized at an early stage of infection, day 3 p.i. A second group was euthanized at the
427 first clinical signs of illness which occurred on day 3 or 4 p.i. in C.MBT-*Rvfs2* mice, and
428 between days 6 and 9 p.i. in BALB/c mice. Finally, BALB/c mice that survived until day 14
429 p.i. were also euthanized. Non infected BALB/c and C.MBT-*Rvfs2* mice were used as
430 controls. The liver and brain were removed and immediately fixed for one week in 10%
431 neutral-buffered formalin for biosafety reasons. Samples from each organ were embedded in
432 paraffin; 4 µm-thick sections were cut and stained with hematoxylin and eosin (HE).
433 Microscope slides were coded for blinded studies, and examined by a qualified veterinary
434 pathologist (GJ). Non-quantitative immunohistochemical detection of the RVFV-infected
435 cells was done using mouse antibodies against the N protein (dilution 1:100) [35]. A rabbit
436 monoclonal antibody (Ref: AB16667, dilution 1:50; Abcam, Paris, France) was used to detect
437 Ki67 antigen. Visualization was performed with the Histofine Simple Stain MAX-PO kit
438 (Nichorei Biosciences Inc., Tokyo, Japan), a labeled polymer prepared by combining amino

acid polymers with peroxidase and secondary antibody which is reduced to Fab' fragment. This visualization procedure allows amplification of the positive signal and limitation of the background staining, especially when using mouse antibodies as for the detection of the RVFV. However, it does not allow quantitative evaluation of positive signals and intensity comparisons between samples.

Primary hepatocyte preparation and infection

Seven to 12 week-old BALB/c and C.MBT-*Rvfs2* male mice were euthanized by cervical dislocation. Suspensions of hepatocytes were prepared as described in Li et al. [36] using Collagenase type IV (PAN Biotech, Worthington, UK) at 100U/ml. Cells were cultured also according to Li et al. [36]. On the day after preparation, hepatocytes were infected with RVFV at an MOI of 3 for 1 hr. At 15, 24, 48 and 60 hours post-infection, the supernatant was collected for virus titration by plaque assay as above. Each condition was done in triplicate (3 wells).

Bone marrow transplantation

Bone marrow cells (BMCs) were collected from both tibias and femurs of 5-6 week-old BALB/c or C.MBT-*Rvfs2* donor male mice. BMCs were resuspended in Hanks'Balanced Salt Solution. After irradiation with one sub-lethal dose of gamma radiation (700 rad), 5-6 week-old BALB/c or C.MBT-*Rvfs2* recipient male mice received ~ 3×10^6 BMCs in 0.15 ml by intravenous injection in the retro-orbital sinus. The extent of reconstitution was evaluated using a semi-quantitative PCR assay based on primers to *Apoptosis-associated tyrosine kinase* (*Aatk*) gene (Forward, 5'-CTACCCCAGGAGGACTGTGTCAGG-3' and reverse 5'-GTCCTCCCCAACAATATCCTGGTGC-3') that maps within *Rvfs2* interval. BALB/c and MBT alleles produce a fragment of 180 bp and 127 bp, respectively. Six weeks after the transplantation, the reconstitution in total peripheral blood of (BALB/c → C.MBT-*Rvfs2*) and (C.MBT-*Rvfs2* → BALB/c) mice was higher than 90%. At that time, bone marrow chimeras

464 were infected intraperitoneally with 100 PFU of RVFV strain ZH548.

465 **Statistical analysis**

466 Statistical analysis was performed using GraphPad Prism 6.0 (GraphPad Software, La Jolla,
467 CA, USA) and R softwares. Mantel-Cox's Logrank test was applied to assess survival curve
468 differences. Two-way ANOVA was used to assess body weight and body temperature
469 differences, with the two factors being the strains and the days post-infection. The p-values
470 shown indicate the significance of the difference between strains. Mann Whitney-U test was
471 used to analyze viral titers in serum and liver.

472

Acknowledgments

The authors are grateful to Daniela Faust for valuable advices in primary hepatocyte preparation. They thank Jean Jaubert and Rashida Lathan for their encouragement and fruitful discussion. The technical assistance of Patricia Flamant, Huot Khun, and Carole Tamietti is gratefully acknowledged. The authors also thank Clémentine Dillard and Marine Perey for technical help during their short stay in the laboratory.

Data Availability Statement

All relevant data are within the paper.

Conflict of Interest

The authors declare no conflict of interest.

Author Contributions

Conceptualization: LB, XM, JJP

Formal analysis: LB, DS, DH, XM, JJP

Funding acquisition: GJ, MF, JJP

Investigation: LB, GJ, DS, DH, OBD, MB, ST, TZDV

Methodology: GJ, AC, MF, XM, JJP

Project administration: JJP

Resources: GJ, MF, XM, JJP

Supervision: XM, JJP

Validation: LB, GJ, MF, AC, XM, JJP

Visualization: LB, GJ, XM, JJP

Writing – original draft: LB, XM, JJP

Writing – review & editing: LB, GJ, DS, DH, MB, ST, TZDV, MF, XM, JJP

Supporting Information

S1 Table. Survival rate and days of death of MBT/Pas and BALB/cByJ 9-12 week-old male mice infected with 10, 100 or 1000 PFU of ZH548 RVFV (dpi : days post-infection).

503 # References

504 1. WHO. Blueprint for R&D preparedness and response to public health emergencies
505 due to highly infectious pathogens 2015. Available from:
506 http://www.who.int/medicines/ebola-treatment/WHO-list-of-top-emerging-diseases/en/.
507 2. Ikegami T, Makino S. The pathogenesis of Rift Valley fever. Viruses. 2011;3(5):493-
508 519. Epub 2011/06/15. doi: 10.3390/v3050493. PubMed PMID: 21666766; PubMed Central
509 PMCID: PMCPMC3111045.
510 3. Pepin M, Bouloy M, Bird BH, Kemp A, Paweska J. Rift Valley fever
511 virus(Bunyaviridae: Phlebovirus): an update on pathogenesis, molecular epidemiology,
512 vectors, diagnostics and prevention. Veterinary research. 2010;41(6):61. Epub 2010/12/29.
513 PubMed PMID: 21188836; PubMed Central PMCID: PMCPMC2896810.
514 4. Busquets N, Xavier F, Martin-Folgar R, Lorenzo G, Galindo-Cardiel I, del Val BP, et
515 al. Experimental infection of young adult European breed sheep with Rift Valley fever virus
516 field isolates. Vector borne and zoonotic diseases (Larchmont, NY). 2010;10(7):689-96. Epub
517 2010/09/22. doi: 10.1089/vbz.2009.0205. PubMed PMID: 20854022.
518 5. Davies FG, Martin V. Recognizing Rift Valley Fever. Veterinaria italiana.
519 2006;42(1):31-53. Epub 2006/01/01. PubMed PMID: 20429078.
520 6. Olaleye OD, Tomori O, Fajimi JL, Schmitz H. Experimental infection of three
521 Nigerian breeds of sheep with the Zinga strain of the Rift Valley Fever virus. Revue d'elevage
522 et de medecine veterinaire des pays tropicaux. 1996;49(1):6-16. Epub 1996/01/01. PubMed
523 PMID: 8881413.
524 7. Bird BH, Khristova ML, Rollin PE, Ksiazek TG, Nichol ST. Complete genome
525 analysis of 33 ecologically and biologically diverse Rift Valley fever virus strains reveals
526 widespread virus movement and low genetic diversity due to recent common ancestry.

527 Journal of virology. 2007;81(6):2805-16. Epub 2006/12/29. doi: 10.1128/jvi.02095-06.
528 PubMed PMID: 17192303; PubMed Central PMCID: PMCPMC1865992.
529 8. Anderson GW, Jr., Slone TW, Jr., Peters CJ. Pathogenesis of Rift Valley fever virus
530 (RVFV) in inbred rats. Microbial pathogenesis. 1987;2(4):283-93. Epub 1987/04/01. PubMed
531 PMID: 3509859.
532 9. Smith DR, Steele KE, Shamblin J, Honko A, Johnson J, Reed C, et al. The
533 pathogenesis of Rift Valley fever virus in the mouse model. Virology. 2010;407(2):256-67.
534 Epub 2010/09/21. doi: 10.1016/j.virol.2010.08.016. PubMed PMID: 20850165.
535 10. Peters CJ, Slone TW. Inbred rat strains mimic the disparate human response to Rift
536 Valley fever virus infection. J Med Virol. 1982;10(1):45-54. Epub 1982/01/01. PubMed
537 PMID: 7130966.
538 11. Anderson GW, Jr., Peters CJ. Viral determinants of virulence for Rift Valley fever
539 (RVF) in rats. Microbial pathogenesis. 1988;5(4):241-50. Epub 1988/10/01. PubMed PMID:
540 3266284.
541 12. Bales JM, Powell DS, Bethel LM, Reed DS, Hartman AL. Choice of inbred rat strain
542 impacts lethality and disease course after respiratory infection with Rift Valley Fever Virus.
543 Frontiers in cellular and infection microbiology. 2012;2:105. Epub 2012/08/25. doi:
544 10.3389/fcimb.2012.00105. PubMed PMID: 22919694; PubMed Central PMCID:
545 PMCPMC3417668.
546 13. Anderson GW, Jr., Rosebrock JA, Johnson AJ, Jennings GB, Peters CJ. Infection of
547 inbred rat strains with Rift Valley fever virus: development of a congenic resistant strain and
548 observations on age-dependence of resistance. Am J Trop Med Hyg. 1991;44(5):475-80.
549 Epub 1991/05/01. PubMed PMID: 2063951.
550 14. Busch CM, Callicott RJ, Peters CJ, Morrill JC, Womack JE. Mapping a Major Gene
551 for Resistance to Rift Valley Fever Virus in Laboratory Rats. The Journal of heredity.

552 2015;106(6):728-33. Epub 2015/11/08. doi: 10.1093/jhered/esv087. PubMed PMID:
553 26546799.
554 15. Gray KK, Worthy MN, Juelich TL, Agar SL, Poussard A, Ragland D, et al.
555 Chemotactic and inflammatory responses in the liver and brain are associated with
556 pathogenesis of Rift Valley fever virus infection in the mouse. PLoS neglected tropical
557 diseases. 2012;6(2):e1529. Epub 2012/03/06. doi: 10.1371/journal.pntd.0001529. PubMed
558 PMID: 22389738; PubMed Central PMCID: PMCPMC3289610.
559 16. do Valle TZ, Billecocq A, Guillemot L, Alberts R, Gommet C, Geffers R, et al. A new
560 mouse model reveals a critical role for host innate immunity in resistance to Rift Valley fever.
561 Journal of immunology (Baltimore, Md : 1950). 2010;185(10):6146-56. Epub 2010/10/13.
562 doi: 10.4049/jimmunol.1000949. PubMed PMID: 20937849.
563 17. Lathan R, Simon-Chazottes D, Jouvion G, Godon O, Malissen M, Flamand M, et al.
564 Innate Immune Basis for Rift Valley Fever Susceptibility in Mouse Models. Sci Rep.
565 2017;7(1):7096. Epub 2017/08/05. doi: 10.1038/s41598-017-07543-8. PubMed PMID:
566 28769107; PubMed Central PMCID: PMCPMC5541133.
567 18. Tokuda S, Do Valle TZ, Batista L, Simon-Chazottes D, Guillemot L, Bouloy M, et al.
568 The genetic basis for susceptibility to Rift Valley fever disease in MBT/Pas mice. Genes and
569 immunity. 2015;16(3):206-12. Epub 2015/01/09. doi: 10.1038/gene.2014.79. PubMed PMID:
570 25569261.
571 19. McGavran MH, Easterday BC. Rift Valley Fever Virus Hepatitis: Light and Electron
572 Microscopic Studies in the Mouse. The American journal of pathology. 1963;42(5):587-607.
573 Epub 1963/05/01. PubMed PMID: 19971024; PubMed Central PMCID: PMCPMC1949706.
574 20. Mims CA. Rift Valley Fever virus in mice. III. Further quantitative features of the
575 infective process. British journal of experimental pathology. 1956;37(2):120-8. Epub
576 1956/04/01. PubMed PMID: 13315887; PubMed Central PMCID: PMCPMC2082563.

577 21. Meegan JM. The Rift Valley fever epizootic in Egypt 1977-78. 1. Description of the
578 epizootic and virological studies. Trans R Soc Trop Med Hyg. 1979;73(6):618-23. Epub
579 1979/01/01. PubMed PMID: 538803.
580 22. Reed C, Steele KE, Honko A, Shamblin J, Hensley LE, Smith DR. Ultrastructural
581 study of Rift Valley fever virus in the mouse model. Virology. 2012;431(1-2):58-70. Epub
582 2012/06/13. doi: 10.1016/j.virol.2012.05.012. PubMed PMID: 22687428.
583 23. Ikegami T. Molecular biology and genetic diversity of Rift Valley fever virus.
584 Antiviral Res. 2012;95(3):293-310. Epub 2012/06/20. doi: 10.1016/j.antiviral.2012.06.001.
585 PubMed PMID: 22710362; PubMed Central PMCID: PMCPMC3586937.
586 24. Kaushansky A, Austin LS, Mikolajczak SA, Lo FY, Miller JL, Douglass AN, et al.
587 Susceptibility to Plasmodium yoelii preerythrocytic infection in BALB/c substrains is
588 determined at the point of hepatocyte invasion. Infection and immunity. 2015;83(1):39-47.
589 Epub 2014/10/15. doi: 10.1128/iai.02230-14. PubMed PMID: 25312960; PubMed Central
590 PMCID: PMCPMC4288894.
591 25. Poyntz HC, Jones A, Jauregui R, Young W, Gestin A, Mooney A, et al. Genetic
592 regulation of antibody responsiveness to immunization in substrains of BALB/c mice.
593 Immunology and cell biology. 2019;97(1):39-53. Epub 2018/08/29. doi: 10.1111/imcb.12199.
594 PubMed PMID: 30152893.
595 26. Anderson GW, Jr., Smith JF. Immunoelectron microscopy of Rift Valley fever viral
596 morphogenesis in primary rat hepatocytes. Virology. 1987;161(1):91-100. Epub 1987/11/01.
597 PubMed PMID: 3499704.
598 27. Raberg L, Sim D, Read AF. Disentangling genetic variation for resistance and
599 tolerance to infectious diseases in animals. Science. 2007;318(5851):812-4. Epub 2007/11/03.
600 doi: 10.1126/science.1148526. PubMed PMID: 17975068.

601 28. Medzhitov R, Schneider DS, Soares MP. Disease tolerance as a defense strategy.
602 Science. 2012;335(6071):936-41. Epub 2012/03/01. doi: 10.1126/science.1214935. PubMed
603 PMID: 22363001; PubMed Central PMCID: PMCPMC3564547.
604 29. Dodd KA, McElroy AK, Jones TL, Zaki SR, Nichol ST, Spiropoulou CF. Rift valley
605 Fever virus encephalitis is associated with an ineffective systemic immune response and
606 activated T cell infiltration into the CNS in an immunocompetent mouse model. PLoS
607 neglected tropical diseases. 2014;8(6):e2874. Epub 2014/06/13. doi:
608 10.1371/journal.pntd.0002874. PubMed PMID: 24922480; PubMed Central PMCID:
609 PMCPMC4055548.
610 30. Roberts KK, Hill TE, Davis MN, Holbrook MR, Freiberg AN. Cytokine response in
611 mouse bone marrow derived macrophages after infection with pathogenic and non-pathogenic
612 Rift Valley fever virus. J Gen Virol. 2015;96(Pt 7):1651-63. Epub 2015/03/12. doi:
613 10.1099/vir.0.000119. PubMed PMID: 25759029; PubMed Central PMCID:
614 PMCPMC4635452.
615 31. El-Akkad AM. Rift Valley fever outbreak in Egypt. October--December 1977. The
616 Journal of the Egyptian Public Health Association. 1978;53(3-4):123-8. Epub 1978/01/01.
617 PubMed PMID: 572393.
618 32. Billecocq A, Gauliard N, Le May N, Elliott RM, Flick R, Bouloy M. RNA polymerase
619 I-mediated expression of viral RNA for the rescue of infectious virulent and avirulent Rift
620 Valley fever viruses. Virology. 2008;378(2):377-84. Epub 2008/07/11. doi:
621 10.1016/j.virol.2008.05.033. PubMed PMID: 18614193; PubMed Central PMCID:
622 PMCPMC2577904.
623 33. Kreher F, Tamietti C, Gommet C, Guillemot L, Ermonval M, Failloux AB, et al. The
624 Rift Valley fever accessory proteins NSm and P78/NSm-GN are distinct determinants of virus
625 propagation in vertebrate and invertebrate hosts. Emerging microbes & infections.

626 2014;3(10):e71. Epub 2015/06/04. doi: 10.1038/emi.2014.71. PubMed PMID: 26038497;
627 PubMed Central PMCID: PMCPMC4217093.
628 34. Yadani FZ, Kohl A, Prehaud C, Billecocq A, Bouloy M. The carboxy-terminal acidic
629 domain of Rift Valley Fever virus NSs protein is essential for the formation of filamentous
630 structures but not for the nuclear localization of the protein. Journal of virology.
631 1999;73(6):5018-25. Epub 1999/05/11. PubMed PMID: 10233964; PubMed Central PMCID:
632 PMCPMC112546.
633 35. Leger P, Lara E, Jagla B, Sismeiro O, Mansuroglu Z, Coppee JY, et al. Dicer-2- and
634 Piwi-mediated RNA interference in Rift Valley fever virus-infected mosquito cells. Journal of
635 virology. 2013;87(3):1631-48. Epub 2012/11/24. doi: 10.1128/jvi.02795-12. PubMed PMID:
636 23175368; PubMed Central PMCID: PMCPMC3554164.
637 36. Li WC, Ralphs KL, Tosh D. Isolation and culture of adult mouse hepatocytes.
638 Methods Mol Biol. 2010;633:185-96. Epub 2010/03/06. doi: 10.1007/978-1-59745-019-5_13.
639 PubMed PMID: 20204628.
640
641

642 **FIGURE LEGENDS**

643 **Figure 1. Representation of the MBT-derived *Rvfs2* region in the congenic C.MBT-*Rvfs2***
644 **strain and its effect on mouse survival.**

645 (A) Haplotype structure of the congenic segment of chromosome 11 in C.MBT-*Rvfs2* (Rvfs2)
646 strain. The MBT-derived segment is depicted in white on the BALB/c chromosome 11
647 background (black). Regions of unknown genotype are depicted in grey. Markers are SNPs
648 from the GigaMUGA array (https://support.illumina.com/downloads/geneseek-ggp-giga-
649 muga-product-files.html) and position are given in bp from mouse Genome Build 37
650 (corrected from [18]). (B) Survival curves of C.MBT-*Rvfs2* and BALB/c male mice infected
651 with 100 pfu IP (Mantel-Cox's Logrank test; $p<0.0001$).

652 **Figure 2. Clinical traits and biochemical parameters of RVFV-infected C.MBT-*Rvfs2***
653 **and BALB/c mice.**

654 (A) Daily body weight variation in C.MBT-*Rvfs2* (Rvfs2) and BALB/c mice after infection
655 with RVFV ZH548 (mean ± SEM). Positive values indicate weight gain (in %) from previous
656 day while negative values indicate weight loss. (B) Body temperature variation in
657 C.MBT-*Rvfs2* and BALB/c mice during the days preceding the death (mean ± SEM). No
658 difference was observed between the two strains (two-way ANOVA, $p=0.69$). (C-D) Alanine
659 aminotransferase (ALT) (C), and aspartate aminotransferase (AST) (D) levels in the serum of
660 C.MBT-*Rvfs2* and BALB/c mice. By day 5 p.i., all C.MBT-*Rvfs2* mice had died. Data are
661 means ± SEM for N= 4-9 mice per day, except for day 8 in BALB/c mice where N=1.

662 **Figure 3. Histopathology and immunohistochemistry analyses of liver from BALB/c and**
663 **C.MBT-*Rvfs2* mice on day 3 p.i.**

664 Three distinct histological profiles were found in 10 BALB/c and 8 C.MBT-*Rvfs2* infected
665 mice. Profile 1: (A) Randomly distributed, multifocal inflammatory lesions (arrowheads) with
666 (B) small well-delimited foci of necrotic/apoptotic hepatocytes associated with neutrophil

667 infiltration. (C) Small clusters of RVFV N protein-positive hepatocytes recognized by
668 immunohistochemistry. Profile 2: (D) Multifocal inflammatory lesions randomly distributed
669 in the liver (arrowheads) with (E) more extensive and severe foci of necrotic/apoptotic
670 hepatocytes than in Profile 1, without inflammatory infiltration. (F) Slightly larger clusters of
671 N-positive hepatocytes observed after immunohistochemistry staining. Profile 3: (G, H)
672 Massive necrosis/apoptosis of hepatocytes, (I) with a strong and diffuse
673 immunohistochemistry staining for RVFV N protein in the parenchyma. None of these lesions
674 were observed in the liver of uninfected BALB/c and C.MBT-*Rvfs2* mice. A, B, D, E, G, H:
675 Hematoxylin and eosin staining; C, F, I: Immunohistochemistry for RVFV N protein.

676 **Figure 4. Hepatocyte proliferation and liver regeneration in BALB/c mice recovering**
677 **from RVFV-induced liver disease.**

678 Liver sections of four BALB/c mice were examined at day 6 post-infection. (A) Rare and
679 randomly distributed lesions in the liver parenchyma are observed (arrows). (B) Small
680 infiltrates of inflammatory cells (primarily neutrophils) associated with focal hepatocyte
681 destruction may be observed in the lesions. Increased mitotic activity is seen among
682 hepatocytes (arrowheads). (C) Immunohistochemistry for RVFV N protein reveals a weak
683 signal, only detected in the small foci identified in hematoxylin and eosin-stained sections
684 (black circles). (D) Immunohistochemistry for Ki67 highlights a marked, diffuse proliferation
685 of the hepatocytes (arrowheads). A, B: Hematoxylin and eosin staining; C:
686 Immunohistochemistry for RVFV N protein; D: Immunohistochemistry for Ki67.

687 **Figure 5. Histopathology and immunohistochemistry analyses of liver and brain from**
688 **moribund BALB/c.**

689 (A-C) Liver from a moribund BALB/c mouse on day 8.5 p.i. displays minimal multifocal
690 inflammatory lesions either randomly distributed in the liver parenchyma (arrowhead) (A) or
691 centered on portal tracts, mostly around bile ducts (arrowhead) (B). Rare RVFV-infected cells

692 are indicated by IHC with antibodies against RVFV N protein (C). (D-I) Brains from
693 moribund BALB/c mice on days 7 to 9 p.i. display different inflammatory and
694 apoptotic/necrotic lesions: subacute leptomeningitis characterized by infiltration of
695 leptomeninges by lymphocytes, plasma cells and neutrophils (D), laminar apoptosis/necrosis
696 of neurons in the cortical outer granular layer (E) with RVFV N protein-positive neurons (F),
697 necrotic/apoptotic foci in different locations of the cerebral grey matter with gliosis (G) and
698 infiltration of neutrophils (inset), and strong signal for RVFV N protein (H-I). Histology and
699 immunohistochemistry results shown are representative of experiments performed on at least
700 4 animals. A, B, D, E, G: Hematoxylin and eosin staining; C, F, H, I: Immunohistochemistry
701 for RVFV N protein.

702 **Figure 6. Production of viral particles and viral proteins in BALB/c and C.MBT-*Rvfs2***
703 **mice on day 3 p.i.**

704 (A) Viremia in RVFV-infected C.MBT-*Rvfs2* (Rvfs2) (N=10) and BALB/c (N=12) mice. (B)
705 Viral titers in liver from C.MBT-*Rvfs2* (N=9) and BALB/c (N=13) mice (C) Western blotting
706 analysis of the liver from BALB/c and C.MBT-*Rvfs2* (Rvfs2) uninfected (N=1) and infected
707 mice on day 3 p.i. (N=2, from the groups of mice analyzed in A and B and identified as b1, b2
708 for BALB/c and r1, r2 for Rvfs2). RVFV-infected AML12 cells were included as a positive
709 control. Proteins were analyzed with antibodies against NSs and N viral proteins, and beta-
710 actin. The molecular weight and positions of the marker bands (middle lane), and NSs, N and
711 β-actin proteins (right lane) are indicated.

712 **Figure 7. Viral replication in primary cultured hepatocytes from BALB/c and**
713 **C.MBT-*Rvfs2* mice.**

714 Virus titer measured in the supernatant of primary cultured hepatocytes, at 15, 24, 48 and 60
715 hr p.i. with RVFV at MOI of 3. Virus titer was significantly higher in C.MBT-*Rvfs2* than in
716 BALB/c hepatocytes at 24 and 48 hr.

Figure 8. Survival curves of chimeric mice generated by reciprocal transplantation of bone marrow cells.

Sub-lethally irradiated C.MBT-*Rvfs2* (Rvfs2, red lines) or BALB/c (black lines) recipient mice received ~ 3×10^6 bone marrow cells from either C.MBT-*Rvfs2* (dashed lines) or BALB/c (solid lines) donor mice on the same day as irradiation. The recipient mice were infected intraperitoneally with 10^2 PFU RVFV six weeks later. Asterisks refer to the comparison between each group and the BALB/c → BALB/c control group (Mandel-Cox's Logrank test; **P<0.01, ***P<0.001).

Fig 1

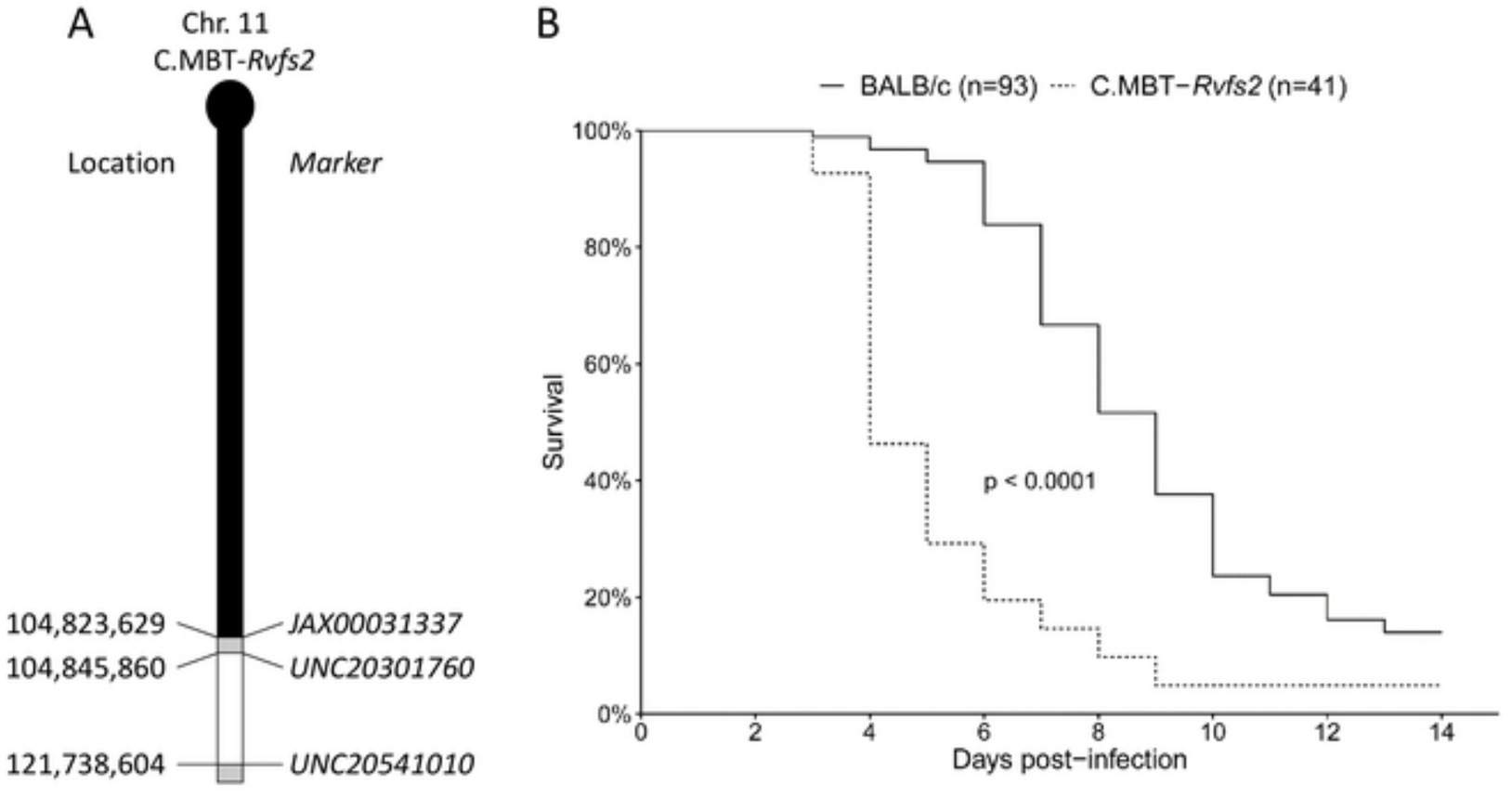

All 8 figures